Clinical and Translational Radiation Oncology 50 (2025) 100877

Contents lists available at ScienceDirect

Clinical and Translational Radiation Oncology

journal homepage: www.sciencedirect.com/journal/clinical-and-translational-radiation-oncology

Determining the gross tumor volume for hepatocellular carcinoma radiotherapy based on multi-phase contrast-enhanced magnetic resonance imaging

Kangning Meng [a,b], Guanzhong Gong [b], Rui Liu [a,b], Shanshan Du [b], Ruozheng Wang [c], Yong Yin [b,*]

[a] Department of Graduate, Shandong First Medical University, Shandong Academy of Medical Sciences, 250117 Jinan, China
[b] Department of Radiation Physics, Shandong First Medical University Affiliated Cancer Hospital, Shandong Cancer Hospital and Institute (Shandong Cancer Hospital), 250117 Jinan, China
[c] Radiotherapy Cencer, Affiliated Cancer Hospital of Xinjiang Medical University, 830011 Urumqi, China

ARTICLE INFO

Keywords:
Multi-phase contrast-enhanced magnetic resonance imaging
Hepatocellular carcinoma
Radiotherapy
GTV determination

ABSTRACT

Purpose: The aim of this study was to quantitatively analyze of the differences in determining the gross tumor volume (GTV) for hepatocellular carcinoma (HCC) radiotherapy using multi-phase contrast-enhanced magnetic resonance imaging (CE-MRI) and provide a reference for determining the GTV for radiotherapy of HCC.
Methods: This retrospective study analyzed 99 HCC patients (145 lesions) who underwent MR simulation. T_1-weighted imaging (T_1WI), contrast-enhanced T_1WI (CE-T_1WI) at 15 s, 45 s, 75 s, 150 s, and 20 min after contrast agent injection were performed, comprising a total of six imaging sequences. The GTVs identified on different sequences were grouped and fused in various combinations. The internal GTV (IGTV), which was the reference structure, was obtained by the fusion of all six sequences. Mean signal intensity (SI), volume, shape, and fibrous capsule (FC) thickness among GTVs were compared.
Results: (1) The mean SI value of $GTV_{\text{-T1WI}}$, $GTV_{\text{-15s}}$-$GTV_{\text{-20min}}$ in patients with transarterial chemoembolization (TACE) was lower by 14.09 % ($GTV_{\text{-T1WI}}$) to 31.31 % ($GTV_{\text{-15s}}$) compared with that in patients without TACE. Except for $GTV_{\text{-T1WI}}$, the differences in SI values between the two groups for other GTVs were statistically significant ($p < 0.05$). (2) The volumes of $GTV_{\text{-T1WI}}$, $GTV_{\text{-15s}}$-$GTV_{\text{-20min}}$ ranged from 32.66-34.99 cm^3. The volume differences between $GTV_{\text{-45s}}$ and the other GTVs were statistically significant ($p < 0.05$), excluding the $GTV_{\text{-T1WI}}$. (3) Compared with the IGTV, the change trend of GTV volume reduction rate is consistent with that of dice similarity coefficients (DSC). (4) In the CE-T_1WI sequences (except for CE-T_1WI$_{\text{-15s}}$), FC measurement was possible in 39.31 % of lesions (57/145), with the largest mean thickness observed at 75 s.
Conclusion: Although single-phase CE-MRI introduces uncertainty in HCC GTV determination, combining different phases CE-MRI can enhance accuracy. The CE-T_1WI$_{\text{-45s}}$ should be routinely included as a necessary scanning sequence.

1. Introduction

Hepatocellular carcinoma (HCC) is one of the most prevalent malignant tumors, with a five-year survival rate of only 18 % [1]. Treatment modalities for HCC include a variety of approaches, such as surgery, transarterial chemoembolization (TACE), radiotherapy, liver transplantation, chemotherapy, and biologically targeted therapy [2]. Advancements in precision radiotherapy technology have significantly improved the efficacy of HCC radiotherapy, making it an indispensable component of comprehensive HCC treatment protocols [3,4].

Accurate determination of gross tumor volume (GTV) is crucial for achieving high-quality irradiation in HCC radiotherapy. The precise delivery of radiation dose is directly influenced by the precision of GTV determination, thereby impacting treatment efficacy and the risk of radiation-induced liver disease (RILD). Therefore, accurate determination of GTV is fundamental assurance for improving the efficacy of radiotherapy and reducing the occurrence of RILD [4,5]. Unclear tumor boundary imaging can influence radiotherapy accuracy for HCC [6,7].

* Corresponding author.
E-mail address: yinyongsd@126.com (Y. Yin).

https://doi.org/10.1016/j.ctro.2024.100877
Received 8 April 2024; Received in revised form 13 October 2024; Accepted 14 October 2024
Available online 22 October 2024

A common approach to determining GTV in HCC radiotherapy is the fusion and registration of computed tomography (CT) and magnetic resonance (MR) images [5,8]. However, CT has certain limitations, such as low soft tissue resolution, unclear tumor boundary imaging, and the large impact of patient respiratory motion, posing challenges in accurately determining the HCC GTV [9]. In contrast, utilizing MR for GTV determination offers advantages such as the absence of ionizing radiation, high soft tissue resolution, detailed anatomical display, and various tumor motion management methods [10,11]. This method has become a key auxiliary method for determining GTV in HCC. Multi-phase contrast-enhanced magnetic resonance imaging (CE-MRI) exhibits distinct characteristics in displaying HCC boundaries at different phases after injecting contrast agent [12]. This study aims to conduct a quantitative analysis to compare the differences in HCC GTV determination using multi-phase CE-MRI. The primary objective is to establish a robust foundation for accurately determining HCC GTV.

2. Materials and methods

2.1. Case selection and general information

This retrospective study included 99 patients diagnosed with HCC who underwent initial radiotherapy at Shandong First Medical University Affiliated Cancer Hospital from August 2021 to March 2023, with a total of 145 lesions examined (detailed information is available in Table 1). Among them, there were 81 males and 18 females, with an age range of 18–82 years and a median age of 58 years. Patients were divided into groups based on whether they had received TACE treatment within the past three months: 41 patients (66 lesions) were included in the TACE group and 58 patients (79 lesions) in the without TACE group.

Inclusion criteria: (1) HCC confirmed by pathological biopsy; (2) first-time radiotherapy; (3) availability of MR contrast-enhanced T_1-weighted imaging (CE-T_1WI) enhanced at 15 s, 45 s, 75 s, 150 s, and 20 min post-contrast agent injection. Exclusion criteria: patients with severe liver cirrhosis.

This study was approved by the Ethics Review Committee of the Shandong Cancer Hospital, and all patients provided informed consent before participation. (Ethical code SDTHEC 201903032).

2.2. Simulation

2.2.1. CT simulation

For 4D-CT simulation achieving in a free-breathing state, all patients were immobilized using a vacuum-lock bag in the supine position with their arms above their heads using a Philips Brilliance Big Bore CT locator (Philips, Amsterdam, Netherlands) [13].

Table 1
Basic information of patients.

	n (%) Total n = 99
Age (y)	
Median (range)	58 (18–82)
Sex	
Male	81 (81.82 %)
Female	18 (18.18 %)
Treatment history	
None	11
Surgery	28
TACE	78
Targeted therapy	14
Targeted therapy combined immunotherapy	22
Systemic chemotherapy	4
Delayed scanning specific time average (range)	
150 s	164.48 (146–185)
20 min	20.45 (16–25)
Tumor diameter (cm)	3.17 ± 1.77

Note: The tumor diameters in the table were measured on CE-T_1WI$_{45s}$ images after contrast agent injection.

2.2.2. MR simulation

After CT simulation, patients remained in the same position for MR simulation using a GE 3.0 T superconducting MR scanner (Discovery 750 W, GE Healthcare, Chicago, IL, USA). Six imaging sequences were obtained using T_1-weighted imaging (T_1WI), CE-T_1WI at 15 s, 45 s, 75 s, 150 s, and 20 min after intravenous injection of a paramagnetic contrast agent (Gadolinium diethylenetriaminepentaacetic acid, Gd-DTPA), as shown in Fig. 1. The CE-T_1WI sequences were named CE-T_1WI$_{15s}$, CE-T_1WI$_{45s}$, CE-T_1WI$_{75s}$, CE-T_1WI$_{150s}$ and CE-T_1WI$_{20min}$.The T_1 plain scan was replaced by T_1WI.

The parameters of the MR scanning sequence were as follows: TR = 5.2 ms, TE = 2.7 ms, FOV = 42–50 cm, matrix = 296 × 256 mm, layer thickness = 3.0 mm, layer spacing = 0 mm. The respiratory state was end-expiration breath-holding (EEBH). The CE-T_1WI sequence used the MR injection system (MEDRAD Spectris Solaris EP, Bayer, Leverkusen, Germany) and Gd-DTPA at a dose of 0.2 mL/kg, administered at a rate of 2 mL/s. After injection of Gd-DTPA, samples were rinsed with 20 mL of normal saline.

2.3. HCC GTV determining and naming

Lesions on T_1WI were defined as masses with low-to-medium signal intensity (SI). CE-T_1WI$_{15s}$ displayed a high SI and a relatively lower SI between CE-T_1WI$_{45s}$ and CE-T_1WI$_{20min}$, as shown in Fig. 2.

All MR images were imported into MIM Maestro software (version 7.1.7, Cleveland, OH, USA). A radiation oncologist determined the GTV manually using T_1WI and CE-T_1WI$_{15s}$-CE-T_1WI$_{20min}$ images, which was subsequently reviewed and revised by two additional radiation oncologists. In cases of disagreement among the three doctors, consensus discussions were held to establish the final determination of GTVs. They were labeled GTV$_{T1WI}$, GTV$_{15s}$, GTV$_{45s}$, GTV$_{75s}$, GTV$_{150s}$ and GTV$_{20min}$, respectively. In addition, a 1 cm^3 region of liver tissue surrounding the lesion, excluding large vessels such as the hepatic artery, hepatic vein, portal vein, and bile duct system, was defined as normal liver tissue, and its SI was measured.

2.4. Fusion and naming of HCC GTV with different sequences

After determining the lesions, GTVs from the same lesion were fused in various combinations-from doubles to sixes-resulting in 57 fused GTVs. The fusions were named based on the following rules: the fused GTV of the T_1WI and CE-T_1WI$_{15s}$ was named the GTV$_{T1WI, 15s}$. The fused GTV of the T_1WI, CE-T_1WI$_{15s}$ and CE-T_1WI$_{45s}$ was named GTV$_{T1WI, 15s, 45s}$. Analogously, the six sequence GTVs were fused into the internal GTV (IGTV), serving as the reference standard.

2.5. Obtaining statistical indicators

Statistical analysis was conducted on multiple aspects, including the mean SI of single-sequence HCC GTVs and normal liver tissue, volumes of all GTVs (63), Dice similarity coefficients (DSC) and volume reduction rates were compared with the IGTV (62). The DSC is defined in Equation (1), and the volume reduction rate is expressed in Equation (2).

$$DSC = \frac{2(|GTV_{-x}| \cap |GTV_{-total}|)}{|GTV_{-x}| + |GTV_{-total}|} \quad (1)$$

$$\textit{the volume reduction rate} = \frac{GTV_{-total} - GTV_{-x}}{GTV_{-total}} \quad (2)$$

Note: GTV$_{-x}$ represents single-sequence GTV or fused GTV.

2.6. Measurement of HCC fibrous capsule (FC) thickness

The CE-T_1WI$_{45s}$-CE-T_1WI$_{20min}$ for all lesions determined whether

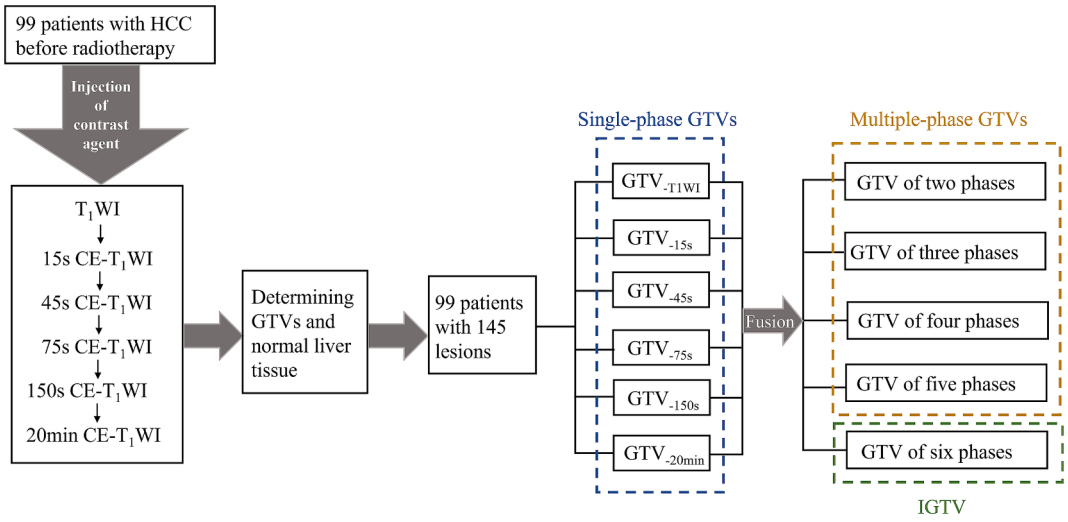

Fig. 1. GTV and IGTV acquisition process.

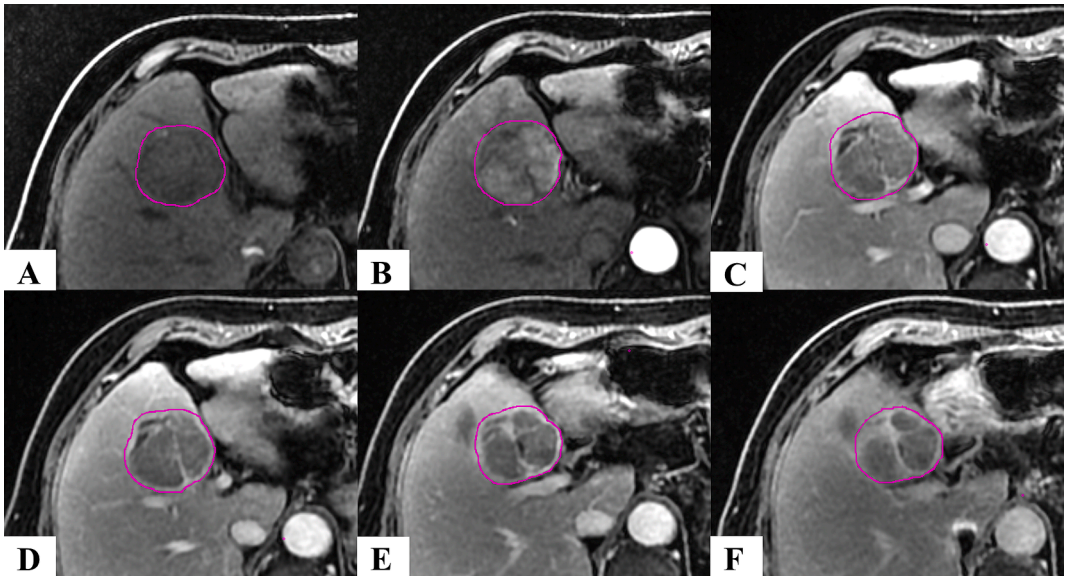

Fig. 2. Schematic diagram of different MR imaging sequences of a patient with HCC A: T_1WI; B-F: CE-T_1WI at 15 s, 45 s, 75 s, 150 s, and 20 min after the intravenous injection of Gd-DTPA.

the presence of FC, and the maximum FC thickness was measured, taking the mean of three measurements as the final FC thickness.

2.7. Statistical analysis

All data was analyzed using IBM SPSS statistical software (version 25.0; Armonk, NY, USA). Wilcoxon tests determined the mean SI of the GTVs and normal liver tissues, volume and FC thickness. Statistical significance was set at $p < 0.05$.

Table 2
Comparison of the mean SI between GTV and normal liver tissue.

	Mean SI of HCC				Mean SI of LIVER			
	Without TACE	With TACE	Difference (%)	*p*-value	With TACE	Without TACE	Difference (%)	*p*-value
GTV_{-T1WI}	407.21 ± 201.04	349.85 ± 141.08	14.09	0.205	456.14 ± 174.75	390.46 ± 154.17	16.82	0.015
GTV_{-15s}	766.34 ± 293.36	526.38 ± 242.52	31.31	<0.001	649.29 ± 283.75	582.87 ± 216.13	11.39	0.270
GTV_{-45s}	953.98 ± 342.69	716.24 ± 255.68	24.92	<0.001	949.62 ± 292.61	881.26 ± 266.13	7.76	0.385
GTV_{-75s}	932.65 ± 343.65	716.79 ± 241.30	23.14	<0.001	930.75 ± 276.90	845.06 ± 276.39	10.14	0.131
GTV_{-150s}	883.68 ± 323.86	705.46 ± 234.91	20.17	0.002	879.76 ± 274.37	799.99 ± 264.05	9.97	0.116
GTV_{-20min}	772.32 ± 254.16	661.28 ± 245.84	14.38	0.010	738.25 ± 236.31	708.47 ± 200.93	4.20	0.621

3. Results

3.1. Comparison of mean SI of GTV and normal liver tissue

3.1.1. Comparison of mean SI of GTV and normal liver tissue in patients without TACE

The mean SIs of the GTV in patients without TACE showed an increasing trend followed by a decreasing trend over time, and GTV_{-45s} had the highest mean SI (953.98 ± 342.69), as shown in Table 2. The mean SI ratios between HCC GTV and normal liver tissue across different sequences were 1.03–1.33. It can be seen that CE-T_1WI$_{-15s}$ had the highest mean SI ratio, as shown in Fig. 3.

The differences in the mean SI of normal liver tissue among the six single-sequence were statistically significant ($p < 0.05$). Furthermore, statistically significant differences were observed in the mean SI of different HCC GTVs ($p < 0.05$), with exceptions for GTV_{-15s} and GTV_{-20min}.

3.1.2. Comparison of mean SI of GTV and normal liver tissue in patients with TACE

The mean SIs of GTV in patients with TACE showed an initial increase and then a downward trend, and the decrease was smaller than patients without TACE. Among them, GTV_{-75s} exhibited the highest mean SI (716.79 ± 241.30), as shown in Table 2. The mean SI ratios of HCC GTV and normal liver tissue for the six single-sequence images were 0.76–0.90. CE-T_1WI$_{-20min}$ had the highest mean SI ratio, as shown in Fig. 3.

The mean SI of normal liver tissue showed statistically significant differences among the other sequences ($p < 0.05$). The mean SI differences between other GTVs were statistically significant ($p < 0.05$), except for GTV_{-45s} and GTV_{-75s}, GTV_{-150s}; GTV_{-75s} and GTV_{-150s}.

3.1.3. Comparison of the mean SI between GTV and normal liver tissue in patients with TACE and those without TACE

In all contrast-enhanced phases, the mean SI value of HCC GTV in patients with TACE group was significantly lower than that in patients without TACE group. The difference in the mean SI value of GTV ranged from approximately 14 % at the minimum between T_1WI and CE-T_1WI$_{-20min}$ to a maximum of 31.3 % in CE-T_1WI$_{-15s}$. The differences in the mean SI value of the normal liver tissue between in patients with TACE group and without TACE group were not statistically significant, except for T_1WI sequence.

The mean SI value of normal liver tissue in patients with TACE group was 4.20 % (CE-T_1WI$_{-20min}$)-16.82 % (T_1WI) higher than patients without TACE group (as shown in Table 2). Among these differences, only the difference observed in T_1WI sequence between the two groups was statistically significant ($p < 0.05$). The mean SI ratios of patients with TACE group were 24.23 %, 51.14 %, 34.84 %, 41.66 %, 37.03 % and 19.68 % lower than those of patients without TACE group at T_1WI and CE-T_1WI$_{-15s}$-CE-T_1WI$_{-20min}$ sequences, respectively. The differences in mean SI ratios between the two groups across different sequences were statistically significant ($p < 0.05$).

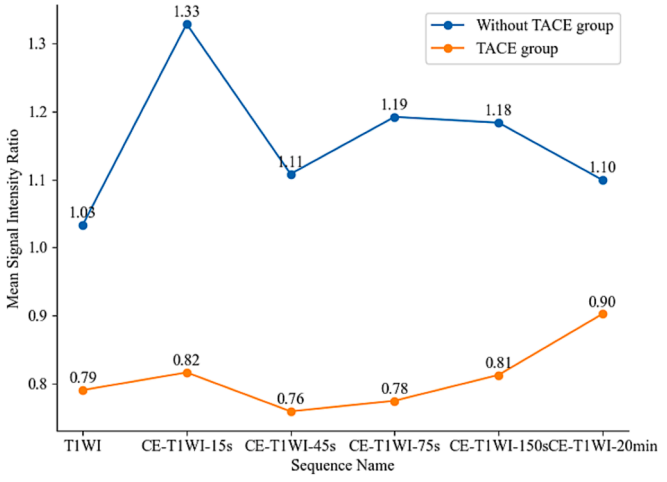

Fig. 3. Trend of the mean SI ratio between GTV and normal liver tissue in patients with TACE and those without TACE.

3.2. Comparison of GTV volumes of different sequences

3.2.1. Comparison of single-sequence GTV volumes

The mean volume of HCC GTV determined through single-sequence MR imaging is the smallest in the GTV_{-20min} (32.66 ± 51.75 cm^3) and largest in the GTV_{-45s} (34.99 ± 53.57 cm^3) ($p < 0.05$). The mean volume of the IGTV is (51.90 ± 72.52 cm^3). The mean volume of a single-sequence GTV was reduced from 43.45 % to 49.11 %, compared to IGTV. The lowest volume reduction rate was observed for GTV_{-45s}, while the highest was observed for GTV_{-20min}, as shown in Fig. 4 and Fig. 5.

The volume differences between GTV_{-T1WI} and GTV_{-15s}; GTV_{-45s} and GTV_{-15s}-GTV_{-20min}; GTV_{-20min} and GTV_{-75s}, GTV_{-150s} were statistically significant ($p < 0.05$). All volume differences between the six single-sequence GTVs and the IGTV were statistically significant ($p < 0.05$).

3.2.2. Comparison of fused GTV volumes

The smallest mean volume among the fused GTVs was observed in $GTV_{-75s, 150s}$ (38.75 ± 58.88 cm^3), while the largest was found in $GTV_{-T1WI, 15s, 45s, 150s, 20min}$ (51.09 ± 71.73 cm^3), see Appendix for details. Fused GTVs showed a volume reduction ranging from 2.64 % to 33.65 % compared with the IGTV. The fused GTV with the smallest volume reduction rate was $GTV_{-T1WI, 15s, 45s, 150s, 20min}$ (2.64 ± 3.30 %), while the largest is $GTV_{-75s, 150s}$ (33.65 ± 16.51 %), see Appendix for details. Compared with the IGTV, the differences between all fused GTVs were statistically significant ($p < 0.05$). Fused GTVs with a reduction rate of less than 5 % are $GTV_{-T1WI, 15s, 45s, 150s, 20min}$ (2.64 ± 3.30 %) and $GTV_{-T1WI, 15s, 45s, 75s, 20min}$ (3.80 ± 4.54 %).

3.3. Comparison of GTV shapes of different sequences

Compared with the IGTV, the DSCs of single-sequence GTV ranged from 0.657 to 0.706. GTV_{-45s} had the largest DSC (0.706 ± 0.152), while GTV_{-20min} displayed the smallest (0.657 ± 0.160). The DSC of the fused GTVs ranged from 0.785 to 0.986, with $GTV_{-T1WI, 15s, 45s, 150s, 20min}$ having the largest DSC (0.986 ± 0.018) and $GTV_{-75s, 150s}$ the lowest (0.785 ± 0.130), see Appendix for details. The change in patterns of all GTV DSCs corresponded to the volume reduction rate pattern. A total of 9 fused GTVs had DSC > 0.95 (Fig. 6).

3.4. Comparison of HCC FC thickness between different sequences

FC was observed in 107 lesions (107/145, 73.79 %). However, ranging from CE-T_1WI$_{-45s}$ to CE-T_1WI$_{-20min}$, FC was detected in only 57 lesions (57/145, 39.31 %). The mean FC thickness measured 0.245 ± 0.061 mm, 0.283 ± 0.067 mm, 0.281 ± 0.079 mm, and 0.274 ± 0.084 mm, respectively, with the maximum at CE-T_1WI$_{-75s}$, as shown in Fig. 7. The differences in HCC FC thickness between CE-T_1WI$_{-45s}$ and CE-T_1WI$_{-75s}$, CE-T_1WI$_{-45s}$ and CE-T_1WI$_{-150s}$, and CE-T_1WI$_{-45s}$ and CE-T_1WI$_{-20min}$ were statistically significant ($p < 0.05$).

4. Discussion

MR has obvious advantages in determining HCC GTV, but there is an issue of insufficient GTV boundary imaging in single-phase MR, and it is uncertain to rely solely on single-phase MR to determine the GTV. This study employed a combined scanning method using T_1 plain scan and multi-phase CE-MRI sequences to optimize the imaging advantages across temporal aspect [14]. Multi-phase T_1WI reflects functional

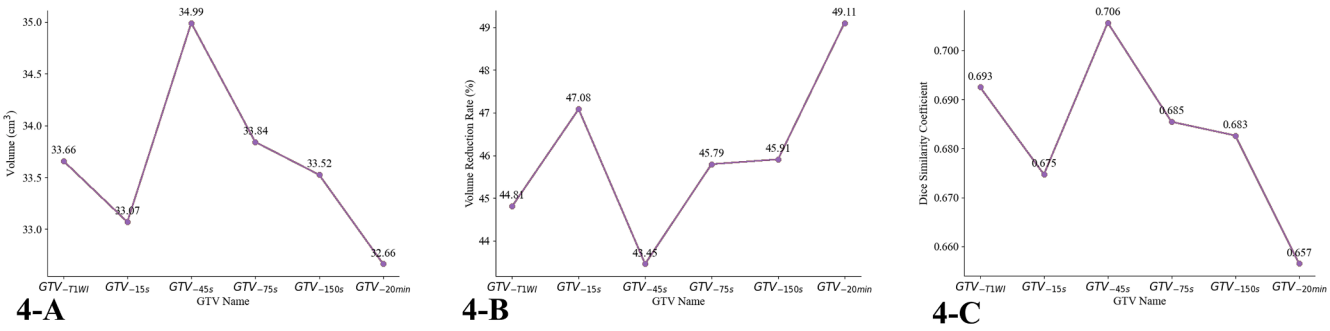

Fig. 4. A. Depicts the volume change trend of a single sequence GTV. B. Illustrates the trend in volume reduction rate of a single sequence GTV compared to IGTV. C. Shows the trend in shape change of a single sequence GTV compared to IGTV.

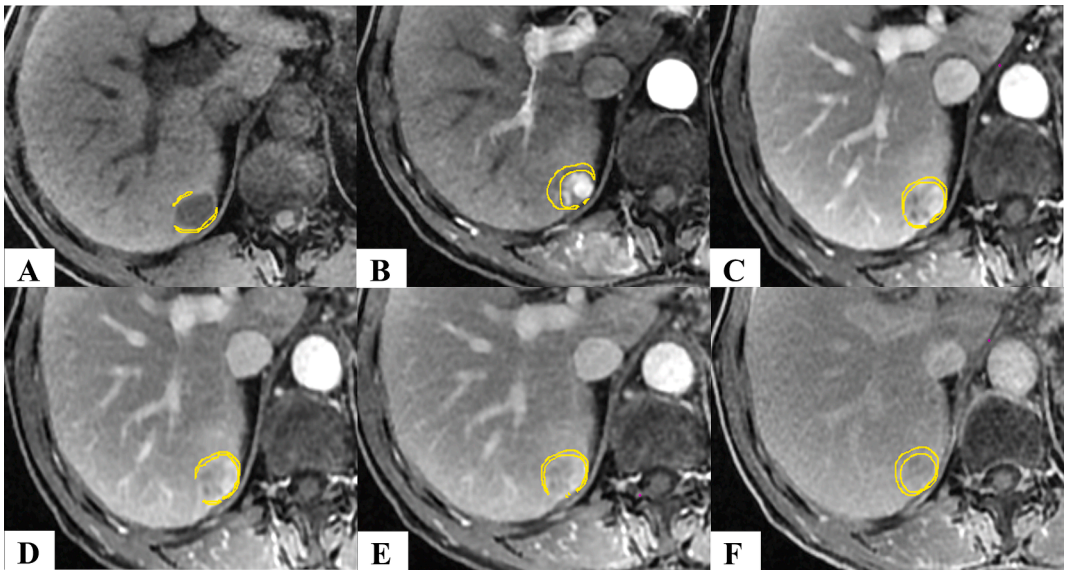

Fig. 5. Diagram illustrating the volume differences of GTV across different MR sequences and IGTV of a HCC patient A: T_1WI; B–F: CE-T_1WI$_{-15s}$-CE-T_1WI$_{-20min}$ after the intravenous injection of Gd-DTPA.

changes in tumor blood vessels and tissues [15]. Further, this procedure can depict imaging and dynamic changes in contrast agents within tumor tissues and FC.

To enhance the local control rate of radiotherapy for HCC, it is necessary to fully consider whether the tumor boundary is fully visualized during GTV determination [16]. Hence, this study used the IGTV derived from six fused MR imaging sequences as the reference standard.

The difference in the blood supply between normal liver tissue and HCC forms the biological basis for multi-phase CE-T_1WI scanning. In this study, the mean SI ratio of the GTV and normal liver tissue in patients without TACE was the highest at CE-T_1WI$_{-15s}$. At the same time, the significant decrease at CE-T_1WI$_{-45s}$ mean SI ratio confirms the typical performance of HCC in "fast in and fast out" in dynamic contrast enhanced MRI (DCE-MRI) [17]. However, the volume of GTV$_{-15s}$ is 47.08 % smaller than that of IGTV. When using GTV$_{-15s}$ as a reference for determining GTV for HCC radiotherapy, it is essential to exercise caution and consider CE-T_1WI images from other sequences.

In this study, the volume of GTV$_{-45s}$ was significantly larger than that of other single-sequence GTVs. During this period, based on the SI of HCC and normal liver tissue in the arterial phase, the SI of HCC increases significantly slower in the portal venous phase. Meanwhile, the surrounding normal liver tissue, influenced by the contrast agent in the portal system, exhibits a significantly faster increase in SI. Consequently, the contrast between the tumor and normal liver tissue decreases. This may be a reason that the GTV$_{-45s}$ is closest in size and shape to the IGTV, despite having the thinnest FC at this time.

During the analysis of the volume and shape of single-sequence GTV, it was observed that both the volume reduction rate and DSC variation amplitude of GTV and IGTV were basically consistent. After injecting contrast agent, the volume of GTV initially exhibited an increase before subsequently decreasing, with the decline commencing at 45 s. This indicates that the penetration and outflow of the contrast agent are in a dynamic process. The turning point observed at 45 s may be attributed to the contrast agent reaching a dynamic equilibrium state, followed by transitioning into an outflow phase. This is supported by the downward trend in HCC SI observed in patients without TACE group.

The SI of HCC after TACE was notably reduced compared with that in patients without TACE. This decline in SI can be attributed to the compromised blood supply to the tumor post-TACE embolization, which restricts the entry of contrast agents into the tumor. Consequently, the tumor exhibits liquefaction and necrosis, resulting in a relatively lower SI. After tumor atrophy and necrosis, the compression of the portal vein system is reduced. Consequently, blood flow in the portal vein increases, resulting in a higher SI of the normal liver tissue than in patients without TACE. At the same time, the SI contrast of tumor boundary imaging after TACE decreased compared with preoperative.

GTV$_{-75s,\ 150s}$ had the highest reduction rates among the fused GTV volumes, displaying a 9.8 % improvement over GTV$_{-45s}$. This finding indicates that fused GTVs can significantly reduce errors caused by single-sequence GTVs. Among the fused GTVs, GTV$_{-T1WI,\ 15s,\ 45s,\ 150s,}$

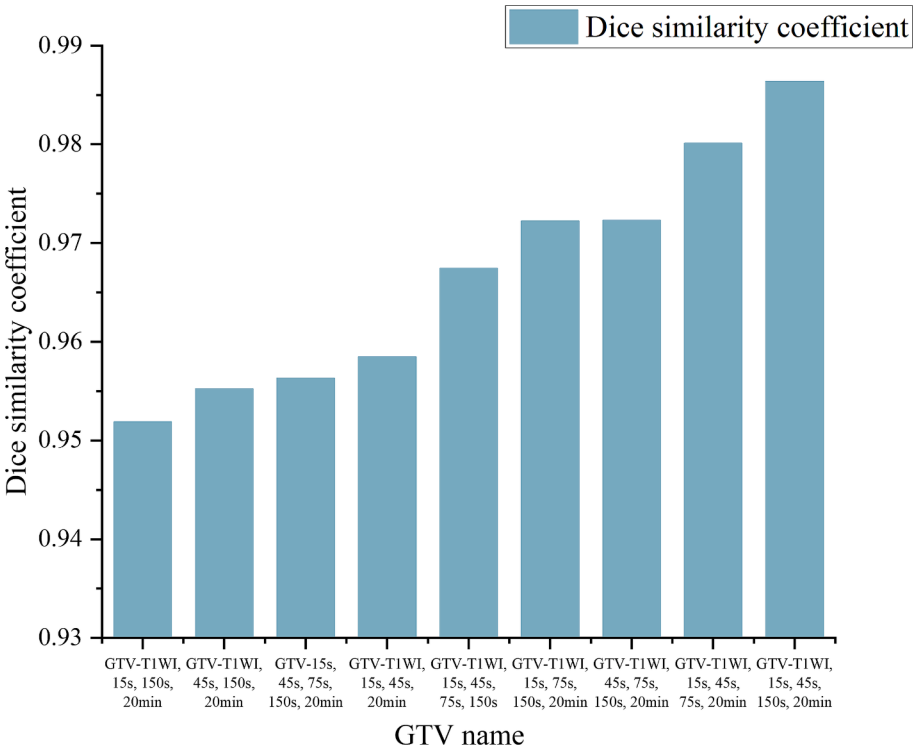

Fig. 6. Fused GTVs with DSC > 0.95.

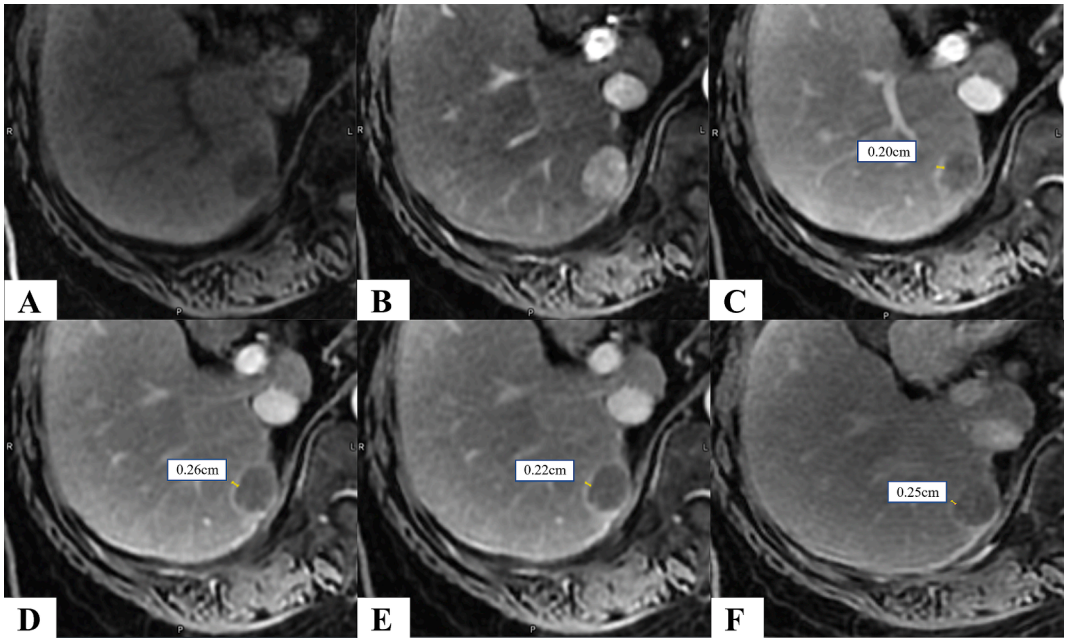

Fig. 7. A HCC patient: measurement of FC thickness across different MR sequences. A: T_1WI; B-F: CE-T_1WI$_{-15s}$-CE-T_1WI$_{-20min}$ after the intravenous injection of Gd-DTPA.

$_{20min}$ had the smallest volume reduction rate (only 2.64 %), while DSC was the largest (0.99), which was closest to the IGTV. This outcome aligns with Duan et al.'s [18] conclusion, indicating that determining the GTV in multi-sequence MR images helps reduce inter-observer variability. The results of this study demonstrated the consistency of the changes in the volume and shape of the fused GTV, confirming that the combination of different phases of MR can significantly make up for the deficiencies of single-phase MR in GTV determination and improve the accuracy of GTV determination, which is consistent with the results of the study by Cheung et al. [4].

In addition, when determining GTV, it was found that when the absolute value of volume change is the same and the tumor volume is smaller, the determination error has a more significant impact on the accuracy of determination.

The novelty of this study lies in the quantitative analysis of differences in determining HCC GTV using multi-phase CE-MRI sequences. We comprehensively considered dynamic changes in SI within HCC GTV and normal liver tissue. This study confirmed that combining different

sequences can improve the accuracy of GTV determination. The main limitation of this study is that it only focused on determining the impact of HCC GTV without examining dosimetry and clinical outcomes in depth. Additionally, multi-phase CE-MRI acquisition extends the patient's scanning time, resulting in decreased tolerance.

In summary, HCC patients who received TACE showed lower tumor SI on MR T_1WI contrast-enhanced scans compared to those who did not receive TACE. The GTV volumes determined from different phases varied significantly. Among the six scanning phases, the CE-T_1WI$_{45s}$ sequence demonstrated clear advantages in depicting tumor volume and shape, while the CE-T_1WI$_{75s}$ sequence exhibited the largest FC thickness. Utilizing multi-sequence MR scans can enhance the accuracy of GTV determination in HCC patients.

Declaration of competing interest

The authors declare that they have no known competing financial interests or personal relationships that could have appeared to influence the work reported in this paper.

Acknowledgments

The authors (KNM, GZG, RL, SSD, RZW and YY) acknowledge financial support for their research work and contribution writing this paper from their sponsors including National Nature Science Foundation of China (Grant Nos. 82072094, 82001902, and 12275162) and Nature Science Foundation of Shandong Province (Grant Nos. ZR2020QH198 and ZR2019LZL017).

Funding

National Nature Science Foundation of China (Grant Nos. 82072094, 82001902, and 12275162) and Nature Science Foundation of Shandong Province (Grant Nos. ZR2020QH198 and ZR2019LZL017).

Appendix A. Supplementary data

Supplementary data to this article can be found online at https://doi.org/10.1016/j.ctro.2024.100877.

References

[1] Jemal A, Ward EM, Johnson CJ, Cronin KA, Ma J, Ryerson B, Mariotto A, Lake AJ, Wilson R, Sherman RL, et al. Annual report to the nation on the status of cancer, 1975-2014, featuring survival. J Natl Cancer Inst 2017;109(9).
[2] Chen W, Chiang CL, Dawson LA. Efficacy and safety of radiotherapy for primary liver cancer. Chin Clin Oncol 2021;10(1):9.
[3] Hong TS, Bosch WR, Krishnan S, Kim TK, Mamon HJ, Shyn P, et al. Interobserver variability in target definition for hepatocellular carcinoma with and without portal vein thrombus: radiation therapy oncology group consensus guidelines. Int J Radiat Oncol Biol Phys 2014;89(4):804–13.
[4] Cheung AL, Zhang L, Liu C, Li T, Cheung AH, Leung C, et al. Evaluation of multisource adaptive MRI fusion for gross tumor volume delineation of hepatocellular carcinoma. Front Oncol 2022;12:816678.
[5] Witt JS, Rosenberg SA, Bassetti MF. MRI-guided adaptive radiotherapy for liver tumours: visualising the future. Lancet Oncol 2020;21(2):e74–82.
[6] Zhao YT, Liu ZK, Wu QW, Dai JR, Zhang T, Jia AY, et al. Observation of different tumor motion magnitude within liver and estimate of internal motion margins in postoperative patients with hepatocellular carcinoma. Cancer Manag Res 2017;9:839–48.
[7] Liu C, Pierce 2nd LA, Alessio AM, Kinahan PE. The impact of respiratory motion on tumor quantification and delineation in static PET/CT imaging. Phys Med Biol 2009;54(24):7345–62.
[8] Dirix P, Haustermans K, Vandecaveye V. The value of magnetic resonance imaging for radiotherapy planning. Semin Radiat Oncol 2014;24(3):151–9.
[9] Khoo VS, Dearnaley DP, Finnigan DJ, Padhani A, Tanner SF, Leach MO. Magnetic resonance imaging (MRI): considerations and applications in radiotherapy treatment planning. Radiother Oncol 1997;42(1):1–15.
[10] Xiao H, Ni R, Zhi S, Li W, Liu C, Ren G, et al. A dual-supervised deformation estimation model (DDEM) for constructing ultra-quality 4D-MRI based on a commercial low-quality 4D-MRI for liver cancer radiation therapy. Med Phys 2022;49(5):3159–70.
[11] Braga L, Guller U, Semelka RC. Pre-, peri-, and posttreatment imaging of liver lesions. Radiol Clin North Am 2005;43(5). 915-927, viii.
[12] Wang W, Z Z: Chinese radiotherapy guidelines for primary hepatocellular carcinoma(2020 edition) [J]. J Clin Hepatol 2021; 37(5): 1029-33.
[13] Chen Y, Gong G, Wang Y, Liu C, Su Y, Wang L, et al. Comparative evaluation of 4-dimensional computed tomography and 4-dimensional magnetic resonance imaging to delineate the target of primary liver cancer. Technol Cancer Res Treat 2021;20. 15330338211045499.
[14] Kim YY, Yeom SK, Shin H, Choi SH, Rhee H, Park JH, et al. Clinical staging of mass-forming intrahepatic cholangiocarcinoma: computed tomography versus magnetic resonance imaging. Hepatol Commun 2021;5(12):2009–18.
[15] Wang XH, Long LH, Cui Y, Jia AY, Zhu XG, Wang HZ, et al. MRI-based radiomics model for preoperative prediction of 5-year survival in patients with hepatocellular carcinoma. Br J Cancer 2020;122(7):978–85.
[16] Yoon SM, Lim YS, Park MJ, Kim SY, Cho B, Shim JH, et al. Stereotactic body radiation therapy as an alternative treatment for small hepatocellular carcinoma. PLoS One 2013;8(11):e79854.
[17] Heimbach JK, Kulik LM, Finn RS, Sirlin CB, Abecassis MM, Roberts LR, et al. AASLD guidelines for the treatment of hepatocellular carcinoma. Hepatology (Baltimore, MD) 2018;67(1):358–80.
[18] Duan J, Qiu Q, Zhu J, Shang D, Dou X, Sun T, et al. Reproducibility for hepatocellular carcinoma CT radiomic features: influence of delineation variability based on 3D-CT, 4D-CT and multiple-parameter MR images. Front Oncol 2022;12:881931.